2016

Photocatalytic degradation of an organophosphorus compound by porous Au- and WO3- modified TiO2

David M. Parker
University of Vermont

Photocatalytic degradation of an organophosphorus compound by porous Au- and WO_3- modified TiO_2

David Parker

University of Vermont

Undergraduate Thesis Project

Advisor: Dr. Christopher C. Landry

ABSTRACT

Organophosphorus (OP) compounds are highly toxic substances that are often used as chemical warfare agents and pesticides. OP pesticides are the most widely used class of pesticide in the world, and due to their ubiquity, the contamination of agricultural runoff by OP pesticides has become a problem of global concern. One of the more attractive solutions that has been proposed is the use of photocatalytic degradation to decontaminate affected water supplies. In the present work, the visible-light photocatalytic activity of a series of porous Au-WO_3-TiO_2 photocatalysts with variable concentrations of Au (0, 1, 3, and 5 weight percent) synthesized using mesoporous SiO_2 as a template was evaluated in the aqueous degradation reaction of an OP agent, dimethyl methylphosphonate (DMMP). The Au and WO_3 were added to the catalysts using sonochemical deposition and incipient wetness impregnation, respectively. The photocatalytic activity of the ternary Au-WO_3-TiO_2 series was compared to that of a WO_3-free series of Au-TiO_2 catalysts with comparable Au loadings. The catalysts were characterized by scanning electron microscopy (SEM), powder x-ray diffractometry (PXRD), and N_2-physisorption. The SEM and N_2-physisorption analyses indicated the Au-TiO_2 and Au-WO_3-TiO_2 particles had high surface areas of 135 $m^2\ g^{-1}$ and 100 $m^2\ g^{-1}$, respectively, with particle diameters of 1-3 µm. No crystalline WO_3 was detected on the WO_3-containing species, indicating the formation of a monolayer of WO_3 on the surface of the TiO_2. The sonochemically deposited gold nanoparticles (NPs) were found to be 3-10 nm in diameter. The photocatalytic degradation of DMMP was monitored by quantitative GCMS analysis. The independent addition of Au NPs or WO_3 to the surface of the TiO_2 did not significantly affect the total degradation of DMMP after 30 hours of irradiation relative to unmodified TiO_2, however the presence of both Au and WO_3 on the surface of the TiO_2 significantly increased the total degradation of DMMP after 30 hours, reaching the detection limit for the 1 and 3 weight percent catalysts. It was found that the photocatalytic activity of the Au-WO_3-TiO_2 catalysts was not significantly influenced by the weight percent Au for the concentrations studied.

INTRODUCTION

Organophosphorus (OP) compounds are a class of compounds that contain a phosphorus-carbon bond. OP species are the active ingredients in a variety of toxic substances, including pesticides and chemical warfare agents (Scheme 1). Synthetic OP compounds include some of the most toxic substances generated by humans. Sarin, the only chemical warfare agent used in a terrorist attack to date, was used twice in Japan in the 1994 and 1995 terrorist attacks that killed 19 people and exposed thousands of others. Among those affected were the rescue workers who were exposed to the vapor that remained in the affected areas. Sarin is considered to be the most likely substance to be used in future instances of chemical terrorism, due to the ease with which it can be produced and distributed and the lethality of the agent itself.[1] The possibility of future sarin attacks has prompted a research initiative to develop materials that can decontaminate affected areas following a sarin attack to prevent further exposure.

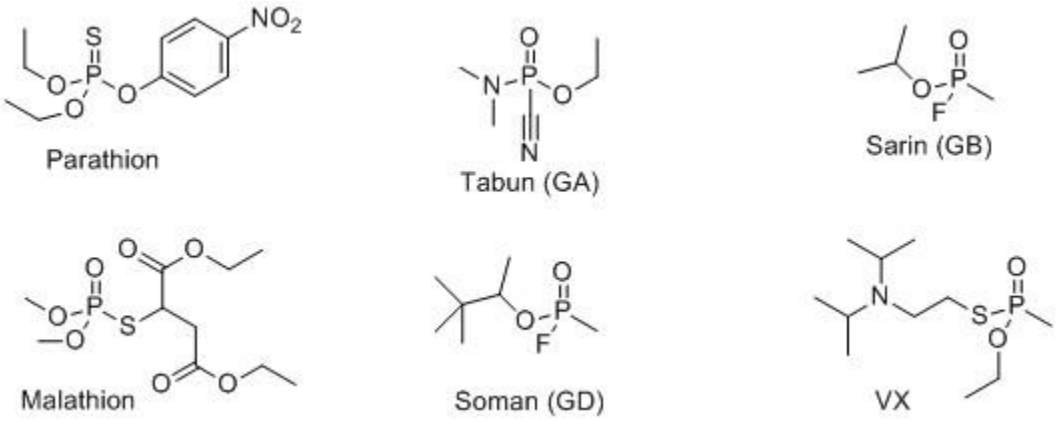

Scheme 1. Common organophosphorus pesticides and chemical warfare agents.

Unlike chemical warfare agents, which are used infrequently and in relatively small quantities, pesticides are regularly used in large quantities over wide areas of agricultural land. OP pesticides are the most widely used class of pesticide, accounting for 38% of pesticide use globally.[2] In recent years, the intimate linkage between agricultural land and watersheds has made contamination of groundwater

by OP pesticides through runoff a global concern. Although chemical warfare agents, such as sarin, are more lethal during acute exposures than pesticides, chronic exposure to pesticides presents a more widespread problem with well documented health complications.[3]

OP compounds are primarily toxic by inhibition of the enzyme acetylcholinesterase. OP compounds act as substrate analogues to acetylcholine and irreversibly bind to the active site of the acetylcholinesterase enzyme, deactivating it.[4] Symptoms of acetylcholinesterase inhibition vary depending on the severity and duration of the exposure and the activity of the agent towards humans. Symptoms can range from lethargy, nausea, tremors, salivation, and miosis (pupil dilation), to more severe symptoms such as convulsions, vomiting, paralysis, and coma.[5] Acute and chronic exposure to certain OP compounds can result in a neurodegenerative disorder called organophosphorus-induced delayed polyneuropathy, which is defined as the delayed development of prolonged locomotor ataxia (reduced muscle control) following one or more exposures to an organophosphorus compound.[6] Organophosphorus-induced delayed polyneuropathy is a condition unrelated to the inhibition of acetylcholinesterase, and is notable because the symptoms associated with the disorder are not apparent for two to three weeks following the neuropathic exposure.[7]

Due to the ubiquitous usage of OP compounds and the potential for ensuing contamination of groundwater, several decontamination routes have been proposed, including bacterial, enzymatic, and catalytic solutions. An ideal catalytic route would consist of a reusable material that utilizes a renewable energy source to drive the decontamination. Heterogeneous photocatalysis has been extensively explored as a solution to OP agent contamination.[8-13] Heterogeneous catalysis describes a system where the catalyst is in a different phase than the substrate. A typical heterogeneous catalytic system is composed of a solid catalyst in a liquid or gaseous medium. A photocatalyst is any catalyst that derives the energy it uses to perform reactions from photons, and a solar photocatalyst is a photocatalyst that uses photons provided by the sun. Metal oxide semiconductors are a common material used in

photocatalysis due to their inherent electronic properties. Titanium dioxide, or titania, in particular has emerged as one of the more promising materials for a functional decontamination system, due to its inherently high stability under irradiation and its low rate of electron/hole recombination relative to other semiconductors.[14] Interest in titania began with the 1972 discovery by Honda and Fujishima that a TiO_2 electrode could be used to generate H_2 and O_2 gas upon illumination in an aqueous solution, otherwise known as water splitting.[15] Following that initial discovery, TiO_2 has seen applications in a variety of fields, including self-cleaning glass surfaces, ceramics, paints, and further research in water splitting.[16-19]

The electronic structure of metal oxide semiconductors is characterized primarily by two electronic bands. The lower energy band, where the majority of the electrons in the material reside, is the valence band. The higher energy band is the conduction band. The energy difference between the two is called the band gap, and each material has a characteristic band gap determined by the electronics of the material. When a material is irradiated by photons with energy equal to or greater

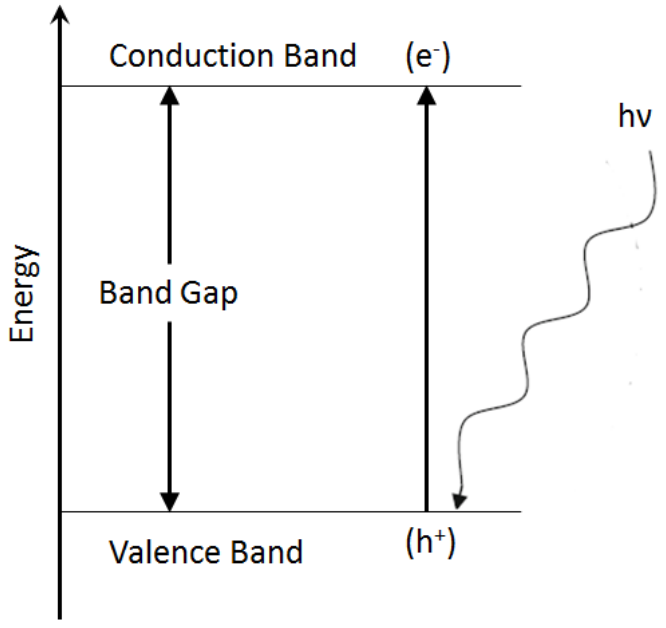

Scheme 2. Formation of e^-/h^+ pair (exciton) on a semiconductor material following photon absorption.

than the energy of the band gap, a negatively-charged electron (e^-) can be promoted from the valence band to the conduction band, leaving a positively charged hole (h^+) in the valence band (Scheme 2). The newly generated electron-hole pair, called an exciton, can then react with species adsorbed on the surface of the material.[18]

In an aqueous environment, such as the one necessary for degradation of OP pesticides in agricultural runoff, dissolved oxygen or water molecules can adsorb to the titania and subsequently react with the photogenerated exciton. The photogenerated hole is a strong oxidizer, and can react with an adsorbed water molecule to form a hydroxyl radical which will then indiscriminately react with the organic species in the solution.[20] Although it is possible for the OP compound to react directly with the exciton when it is adsorbed on the surface of the titania,[11] in a dilute aqueous solution of the contaminant, degradation is more likely to occur through a hydroxyl radical mechanism.[21]

Although titania offers an advantage over other metal oxide semiconductors in the field of photocatalysis due to its high photostability and low rate of electron/hole recombination, there are disadvantages associated with it as well. The primary disadvantage is the large band gap of titania, which is about 3.2 eV,[22] and corresponds to the energy of photons in the ultraviolet region of the electromagnetic spectrum. The bandgap presents an obstacle for applications of TiO_2 as a solar photocatalyst because UV radiation only accounts for 3-5% of the total energy present in solar radiation. Additionally, although titania generally has a lower rate of electron/hole recombination than other metal semiconductor materials, there is still considerable room for improvement. A lower rate of e^-/h^+ recombination means the likelihood of an exciton reacting with a species adsorbed on the surface of the material is higher, which in turn increases the efficiency, or quantum yield, of the catalyst in a reaction system. An ideal photocatalyst would have a quantum yield of 1, a system in which one reaction is performed for each photon absorbed by the material. A great deal of the research performed on titania-based materials is oriented towards improving the quantum yield in chemical systems.

Doping is one of the more promising techniques being explored in the effort to optimize titania for solar photocatalysis. Doping refers to the incorporation of a small quantity of another substance, such as a nonmetal anion,[14,23-24] another transition metal oxide,[25-29] or a noble metal such as gold, platinum, or palladium.[12,30-31] One of the purposes of doping is to provide the material with additional electronic states that can be used to "trap" the excited electrons before allowing them to recombine with the hole (Scheme 3). Depending on the dopant and the conditions used during the synthesis, however, dopants can also facilitate charge carrier recombination and actually decrease the efficiency of the photocatalyst. Dopants can be used to narrow the band gap of titania by introducing intra-gap electronic states that allow for movement of electrons from electronic states other than those present in pristine TiO_2.[32-33]

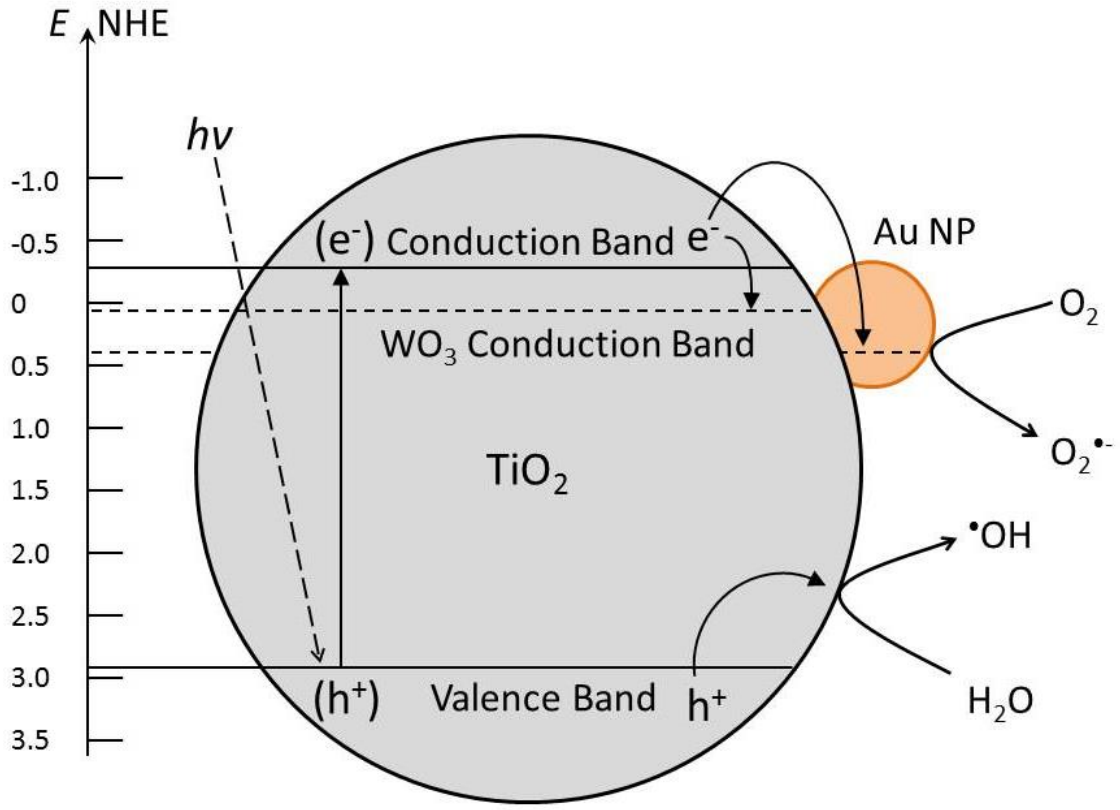

Scheme 3. Au NP and WO_3 codoped TiO_2 particle. Adsorbed O_2 and H_2O can react with a photogenerated e^-/h^+ pair to form a superoxide radical and hydroxyl radical, respectively.

Chemistry in a heterogeneous catalytic system occurs at the interface between the two phases present. For a solid catalyst in a liquid substrate, a large surface area is desirable because it results in more interaction between the catalyst and substrate, typically resulting in more reactions and thus a more active catalyst. An ideal photocatalyst would allow each exciton to react with an adsorbed species, with an overall quantum yield of one (one reaction performed for each photon absorbed by the material). In order to maximize the number of excitons that react rather than recombine, the number of adsorbed species on the surface of the catalyst also needs to be maximized, which can be done by modifying the surface to increase the adsorption potential of a species by modifying the surface acidity of the catalyst[34] or by increasing the surface area of the material.

The synthesis of high surface area materials can be broadly divided into two categories, the more conventional soft templating techniques, and hard template techniques otherwise known as nanocast synthesis. While soft templating techniques incorporate structure-directing agents called surfactants into the synthesis of a material, nanocast syntheses utilize an existing high-surface area material as a framework to which another material is added. The 1992 discovery by the Mobil Company of highly ordered mesoporous silica (SiO_2), which contain systems of interconnected pores between 2 and 50 nm in diameter and can have surface areas in excess of 1000 $m^2\ g^{-1}$, opened the door to nanocasting techniques for the synthesis of high surface area non-silica microstructures.[35] The nanocast synthesis often utilizes ordered silica as a hard template. The second material adopts a structure defined by the pore structure of the silica, which can then be removed leaving a structured material with high surface area (Scheme 4). The nanocast synthesis can be performed using alternative templates, such as high surface area carbon materials, but silica is commonly used as a template on account of the wide variety of nanostructures that can be created from it and the ease with which it can be preferentially removed from a complex through treatment with either base or hydrofluoric acid.[36] Scheme 4 displays a nanocast synthesis for a highly ordered mesoporous silica, MCM-41, but amorphous silica templates,

such as the one used in the present work, feature less symmetry and a more highly connected pore structure than MCM-41.

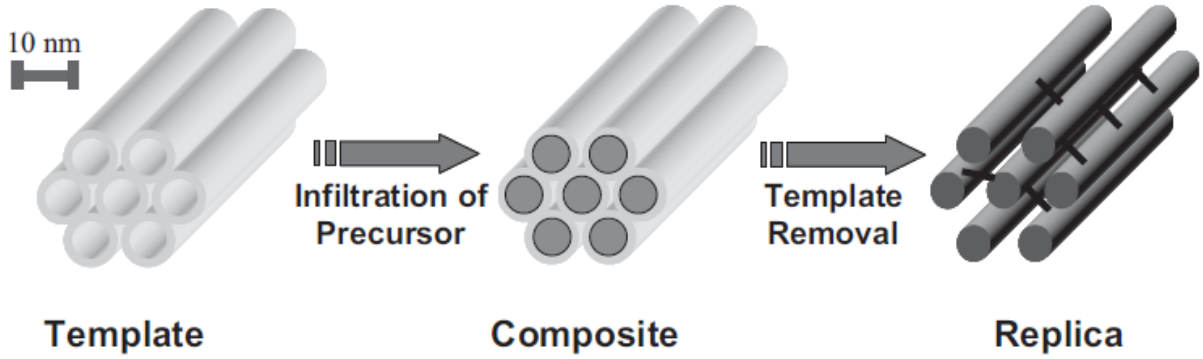

Scheme 4. General outline of a nanocast synthesis using ordered mesoporous silica MCM-41.

The present work focuses on the effects of two materials codoped onto a titania substrate, tungsten oxide (WO_3) and gold nanoparticles (Au NPs). WO_3 has been shown to increase the photocatalytic activity of TiO_2 toward a variety of substrates.[26-27, 37-38] Several mechanisms by which this increase occurs have been proposed. A prevailing theory is that the additional WO_3 electronic states, specifically the conduction band, which has a lower energy than the conduction band of TiO_2, can serve as charge transfer locations to trap photoexcited electrons, in turn preventing the recombination of e^-/h^+ pairs while the hole remains in the TiO_2.[39] Additionally it has been shown that the addition of WO_3 to TiO_2 increases the surface acidity, which allows substrates to adsorb more strongly to the material and has been shown to increase photocatalytic activity.[25, 34] In an aqueous system, this would allow for a higher rate of production of reactive hydroxyl radicals that can then react with the desired substrate. Other studies have indicated that the addition of WO_3 to TiO_2 can redshift the absorption energy of the TiO_2 to the visible region of the electromagnetic spectrum.[27, 37, 40]

The photocatalytic activity of titania can also be improved through the deposition of Au NPs on the surface of the TiO_2,[30, 41-42] although the improvement is largely dependent on the concentration,

shape, and size of the Au nanoparticles.[43] The method of addition can be adjusted to change the morphology of the Au NPs. One of the traditional synthetic procedures, called photodeposition, involves the addition of a gold precursor solution containing oxidized gold species, typically Au (III), to a metal oxide semiconductor that is then irradiated by photons with energy greater than or equal to the band gap of the material. The photoexcited electron from the semiconductor material then reduces the gold species in the precursor molecules adsorbed on the material, resulting in the growth of gold nanoparticles on the surface of the metal oxide. More recently, sonochemical cavitation has been used to anchor noble metal nanoparticles on a variety of substrates, including silica and titania.[44] Au NPs anchored on TiO_2 through a sonochemical deposition technique were shown to increase the photocatalytic efficiency of the TiO_2.[41]

Although there have been a number of studies performed on singly-doped TiO_2, codoped TiO_2 (ternary) compounds have received considerably less attention. In a study performed by Iliev et al.[45] on ternary Au-WO_3-TiO_2 compounds, the authors found that the mineralization rate of oxalic acid by the ternary compound was 3.2 times higher than for unmodified TiO_2, and 2.2 times higher than for WO_3-TiO_2. A conclusion shared by the various studies performed on ternary Au-WO_3-TiO_2 compounds is that the manner of synthesis can have dramatic effects on the final photocatalytic activity of the material.[45-47] To the author's knowledge, no studies have yet been performed on the visible light photocatalytic degradation of an OP compound by a ternary Au-WO_3-TiO_2 species. The purpose of the present work was to investigate how the addition of WO_3 affected the visible light photocatalytic activity of variable weight percent loadings of Au NPs on TiO_2 toward an OP compound, dimethyl methylphosphonate (DMMP).

EXPERIMENTAL

Materials. Materials used in the following synthesis were purchased from Sigma-Aldrich and used without further purification unless otherwise indicated. The gold precursor was a 25.84 mM aqueous solution of 1.0177g $HAuCl_4 \cdot 3H_2O$ (Fisher Scientific) in 100 mL deionized H_2O.

Synthesis. The photocatalysts were prepared using a nanocasting technique, with disordered mesoporous silica microspheres as the template. The procedure used to generate the silica spheres was adapted from the literature.[48] In a typical synthesis, a mixture of 198 grams of deionized H_2O, 22 grams of concentrated HCl, and 55.5 grams of EtOH were added to a 500 mL Erlenmeyer flask. Then, 9.0 grams of cetyltrimethylammonium bromide (CTAB) was added, followed by 20 grams of tetraethyl orthosilicate (TEOS) upon dissolution of the CTAB. After five minutes of stirring, 23.8 grams of 0.5 M NaF solution was added, and after about 80 seconds of stirring the solution became opaque and was immediately transferred into a Teflon bottle and placed in an oven at 373 K for 100 minutes. After heating, the bottle was removed and cooled in an ice bath. The solution was then filtered, and the filtered particles were washed with water then ethanol. The particles were allowed to dry in air and then were calcined using the following program: samples were heated from 298 K to 723 K at 2 K/min, held at 723 K for 240 min, heated to 823 K at 10 K/min, then held at 823 K for 480 min.

The titania microspheres were synthesized using a modified method previously described by Leitner et al.[49] The silica microspheres were impregnated with an excess of a 50% (v/v) solution of titanium isopropoxide (TTIP) in EtOH by shaking for 20 hours. The excess solution was removed through centrifugation and the residual solution was removed by drying the sample overnight in a 353 K convection oven. The sol-gel reaction of the titanium isopropoxide present in the silica microspheres was initiated by the addition of excess 50% (v/v) solution of H_2O in EtOH, which was left to shake for 3 hours. The impregnation and sol-gel steps were repeated once to ensure the structure of the TiO_2 would

withstand etching, and then the particles were calcined using the same program described for the silica microspheres.

The gold nanoparticles were added to the TiO_2-SiO_2 microspheres using a sonochemical method adapted from DePuccio et al.[50] The TiO_2-SiO_2 particles were dispersed in 150 mL of water and stirred for 15 minutes. A variable amount of chloroauric acid trihydrate solution (1.0177 g $HAuCl_4 \cdot 3H_2O$ in 100 mL H_2O) was added under vigorous stirring to achieve loadings of 0, 1, 3, and 5 wt. % gold nanoparticles. After 45 minutes of stirring, the solution was submersed in a water bath-type sonicator (Branson 2510, 40 kHz, 130 W) for an additional 45 minutes. Throughout the sonication procedure, concentrated ammonium hydroxide solution (28.0-30.0% NH_3 basis) was added dropwise to the solution so that the molar ratio of $HAuCl_4$ to NH_4OH was 1:100. The product was filtered and rinsed with deionized H_2O, dried, ground, and calcined at the following program: heat from 298 K to 673 K at 1 K/min, followed by a 240 minute hold at 673 K. Following the deposition of gold nanoparticles, the SiO_2 template was removed from the particles by three sequential three hour washes with excess 2 M NaOH solution at room temperature.

The WO_3 (4% w/w) was added to the catalysts using an incipient wetness preparation after the Au NP addition step and the SiO_2 removal, both of which were performed in basic solutions, due to the instability of WO_3 in basic solutions. The weight percent used was determined after a literature review[45-47] indicated that 4 weight percent of WO_3 relative to TiO_2 would be optimal. Ammonium metatungstate hydrate (AMT, molecular weight 2956.30 g/mol, formula $(NH_4)_6H_2W_{12}O_{40}$) was added using the incipient wetness method. A quantity of AMT was dissolved in deionized water so that the volume of solution containing 4 weight percent WO_3 equaled the pore volume of the Au-TiO_2 particles as determined by N_2 physisorption. The solution was added dropwise to the particles under manual stirring over a period of 10 minutes, after which the particles were stirred for an additional 15 minutes. The particles were dried

at room temperature, with periodic stirring, and then were calcined at the following program: heat from 298 K to 693 K at 1 K/min, followed by a 120 minute hold at 693 K.

Characterization. Nitrogen physisorption was performed at 77 K on a Micromeritics Tristar 3000 porosimeter. Samples were degassed at 373 K under a stream of ultrahigh purity N_2 (Airgas). Surface areas were calculated using the BET method, and pore size distributions were calculated using the BJH method. Powder X-ray diffraction (PXRD) measurements were performed on a Rigaku MiniFlex II diffractometer using Cu Kα (0.15418 nm) radiation at 30 kV and 15 mA. Scanning electron microscopy (SEM) was performed on a JEOL JSM-6060 SEM at 20 kV. IR spectroscopy was performed on solid samples to confirm removal of the silica framework during synthesis on a Shimadzu IRAffinity-1FT-IR spectrometer equipped with an attenuated total reflectance accessory.

Photocatalysis. The photocatalytic activity towards dimethyl methylphosphonate (DMMP) of the 0, 1, 3, and 5 wt. % Au-WO_3-TiO_2 catalysts were evaluated under the irradiation of a 75 W xenon arc lamp (Photon Technology International, Ushio UXL-75E). Photocatalytic experiments were performed in a water-cooled beaker with 100 mL of aqueous solution containing 0.25 g/L dimethyl methylphosphonate (DMMP) and 100 mg/L catalyst. The DMMP was quantified by gas-chromatography mass-spectrometry (GCMS) following a liquid-liquid extraction procedure with chloroform as the extraction solvent. The GCMS instrument was an Agilent 6890 Series GC with an HP-5 crosslinked 5% phenyl methyl siloxane column of dimensions 30m x 0.32 mm x 0.25 µm film thickness equipped with an Agilent 5973 Network MS. The extraction was performed as follows: 5 mL of the reaction solution was removed and filtered to remove the catalyst. An extraction standard of diethyl methylphosphonate (DEMP, 250 µg/mL) was added, and the liquid-liquid extraction was performed two times in a separatory funnel. A GCMS standard of diethyl ethylphosphonate (DEEP, 250 µg/mL) was added to 5 mL of the chloroform containing the DMMP and DEMP and 1 µL of the solution was manually injected into the GCMS. The

GCMS was operated in split mode with a split ratio of 10.5:1, an inlet temperature of 523 K and the following oven program: starting temperature of 373 K, increased to 423 K at 5 K min^{-1}, and then increased to 493 K at 20 K min^{-1}. Scheme 5 displays the photocatalytic reactor setup.

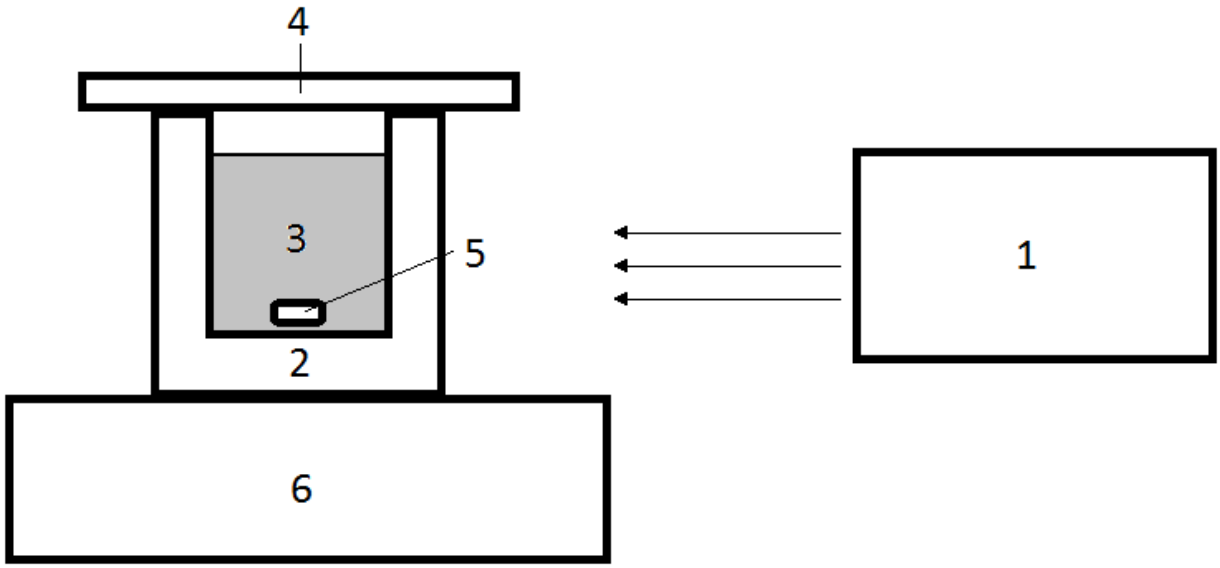

Scheme 5. Photocatalytic reactor layout (1) 75W Xe short arc lamp (2) Borosilicate water-cooled reaction vessel (3) reaction mixture (4) UV-filter (5) stir bar and (6) stir plate.

RESULTS AND DISCUSSION

Catalyst Porosity Analysis by N_2 Physisorption

The specific surface area, pore volume, and pore size distribution for each catalyst were determined by N_2-physisorption using the Brunauer-Emmett-Teller (BET) and Barrett-Joyner-Halenda (BJH) methods, respectively (Table 1). Figure 1 displays characteristic isotherms for the mesoporous silica template, TiO_2-SiO_2, Au-TiO_2 catalysts, and Au-WO_3-TiO_2 catalysts. The BET surface area calculations are performed on the low partial pressure section of the isotherm, which chemically corresponds to the establishment of a monolayer of N_2 molecules adsorbed on the surface of the material.[51] A steeper slope at low partial pressures is indicative of a higher surface area. In Figure 1, the

SiO_2 template has a higher surface area than the final catalyst materials, as indicated by the sharp increase in the low partial pressure region of the isotherm relative to the Au-TiO_2 and Au-WO_3-TiO_2 isotherms. The pore volume calculations are performed on the central region of the isotherm, in the region called the hysteresis loop. The hysteresis loop is associated with capillary condensation of N_2 in mesoporous structures, and the application of the BJH calculation allows for the determination of the pore size distribution.[52] The pore volume of a structure is determined using the total volume adsorbed at the maximum partial pressure. In the catalyst isotherms shown in Figure 1, the isotherm shows an increase in volume adsorbed at high partial pressures, a feature indicative of surface porosity, or the existence of textural features on the surface of the catalyst particles.

The specific surface area of each catalyst decreased with successive steps in the synthetic procedure. The mesoporous silica template had a surface area of 595 $m^2 g^{-1}$, while the Au-TiO_2 and Au-WO_3-TiO_2 catalysts had average surface areas of 135 $m^2 g^{-1}$ and 102 $m^2 g^{-1}$, respectively. The surface area decrease between the Au-TiO_2 and Au-WO_3-TiO_2 series can be attributed to the additional calcination performed during the WO_3 addition step or to pore blockage by WO_3 species. However, the surface area difference between the Au-TiO_2 and the Au-WO_3-TiO_2 catalysts was not considered significant enough to influence the photocatalytic activity displayed by the two series. Surface area is measured in units of $m^2 g^{-1}$, which will result in an apparent decrease in surface area when the density of a catalyst is increased through the addition of a higher density material like WO_3.

Table 1: N_2 physisorption data, diameter of gold NPs, and anatase crystallite sizes for porous Au-TiO_2 and Au-WO_3-TiO_2 catalysts

Catalyst	S_{BET} ($m^2 g^{-1}$)	V_{pore} ($cm^3 g^{-1}$)	d_{pore} (Å)	*Au Diameter (nm)*	*TiO_2 Crystallite Size (nm)*
0Au-TiO_2	146	0.25	64	-	6.9
1Au-TiO_2	133	0.23	64	3.3	6.9
3Au-TiO_2	136	0.25	65	5.9	7.0
5Au-TiO_2	127	0.23	65	5.2	7.2
0Au-WO_3-TiO_2	104	0.22	85	-	7.6
1Au-WO_3-TiO_2	103	0.22	84	10.2	7.1
3Au-WO_3-TiO_2	101	0.20	87	6.7	7.1
5Au-WO_3-TiO_2	100	0.20	85	5.9	7.1

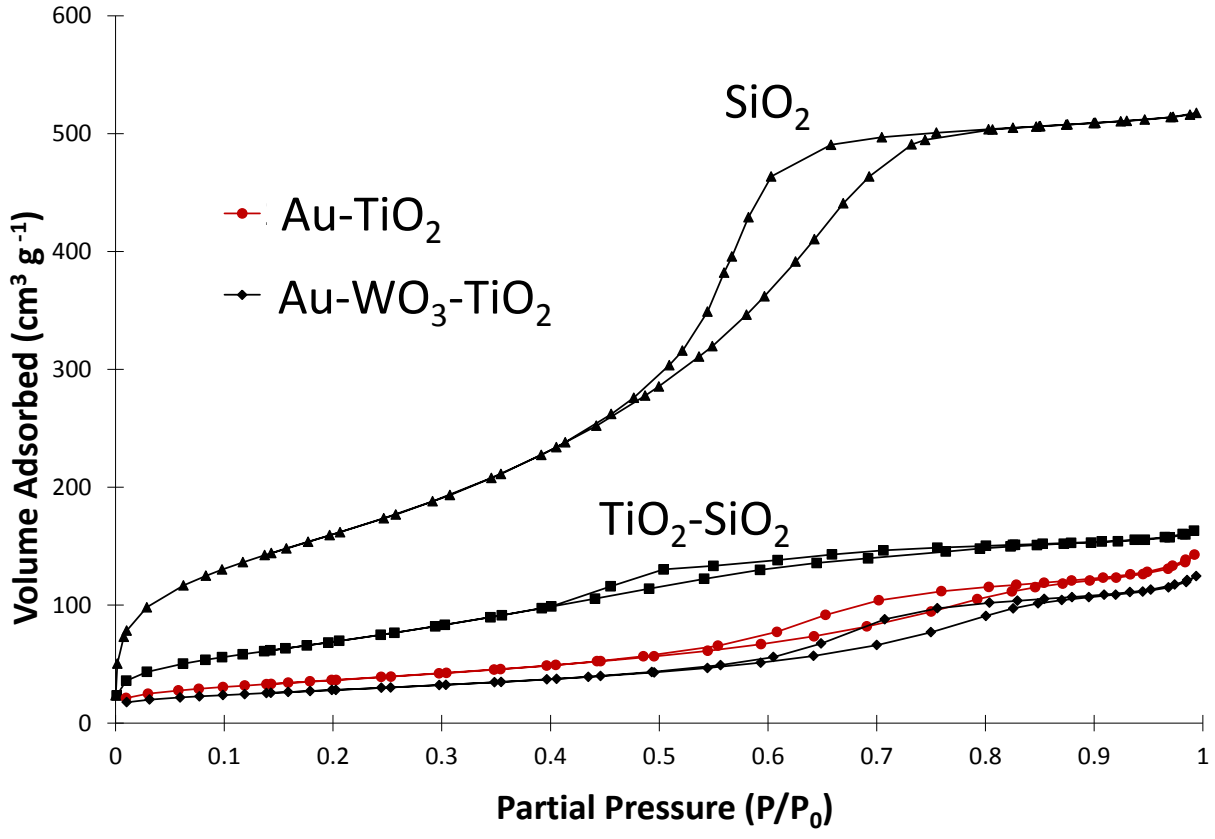

Figure 1. N_2-physisorption isotherms for the mesoporous SiO_2 template, TiO_2-SiO_2 compound, Au-TiO_2, and Au-WO_3-TiO_2 catalysts.

Particle Morphology Analysis by Scanning Electron Microscopy

Particle morphology was observed using scanning electron microscopy (SEM). Figure 2 displays the mesoporous silica template, the titania-silica binary material, a typical Au-TiO_2 catalyst, and a typical Au-WO_3-TiO_2 catalyst. While the silica template and the titania-silica compound was characterized by smooth spherical particles with diameters of 1-3 μm, upon removal of the silica framework the surface of the TiO_2 particles appeared more rough and asymmetrical while retaining the same range of diameters (1-3 μm) as the SiO_2 and TiO_2-SiO_2 materials. The surface texturization shown in the SEM images is consistent with the surface porosity features in the N_2-physisorption isotherms for each catalyst. However, some of the surface features and the smaller particles shown in panels B, C, and D of Figure 2 may have been caused by the separate coprecipitation of TiO_2 during the nanocast synthesis by excess TTIP that was not removed after the impregnation of the SiO_2 μ-spheres. Additional analysis by high-resolution transmission electron microscopy (HR-TEM) would allow the composition of the SEM images to be confirmed. The efficiency of the impregnation of the TiO_2-SiO_2 compound could also be quantified through the use of ^{29}Si nuclear magnetic resonance (^{29}Si-NMR). The surface of a silica compound is characterized by Si—O—H bonds, which can be detected using ^{29}Si-NMR. The efficiency of TTIP loading on the silica μ-spheres could be determined through the decrease in the Si—O—H signal as the surface bonds are converted to Si—O—Ti bonds. The additional HR-TEM and ^{29}Si-NMR data would allow for improvement of the synthesis of the TiO_2 catalyst μ-spheres.

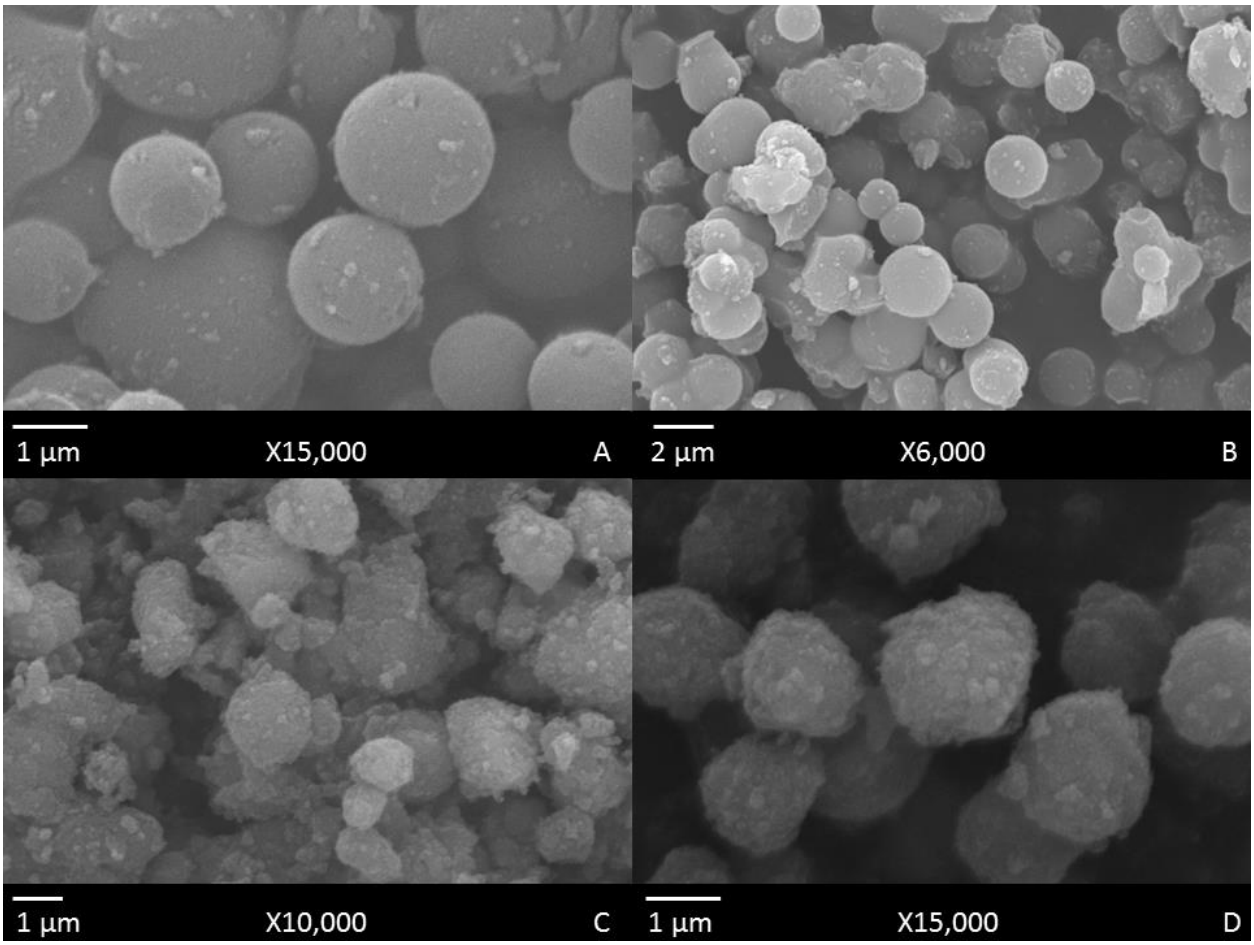

Figure 2. SEM images of (A) mesoporous SiO_2 template (B) TiO_2-SiO_2 composite (C) Typical Au-TiO_2 catalyst and (D) Typical Au-WO_3-TiO_2 catalyst.

X-ray Diffractometry Analysis

The x-ray diffraction patterns of the catalysts are shown in Figure 3. Titania can exist in three crystal phases, anatase, rutile, and brookite. Anatase is typically the most photocatalytically active phase,[53] while rutile is the thermodynamically most stable phase. Although no consensus exists as to why anatase is more photocatalytically active, proposed explanations include longer exciton lifetimes in anatase than in rutile, which allows the photogenerated species more time to react with adsorbed molecules, favorable charge carrier transport properties, allowing non-surface photogenerated excitons

to travel farther to reach adsorbed species on the surface in anatase than in rutile, and favorable surface properties on anatase that allow molecules to adsorb more easily and react with photogenerated e^-/h^+ pairs.[54] During heat treatment, synthesized anatase phase TiO_2 will tend to transition into the thermodynamically more stable rutile phase. For all the catalysts synthesized, the TiO_2 diffraction pattern was consistent with that of anatase, with the peaks appearing at 25.4°, 38.1°, 48.1°, 54.4°, and 62.7° corresponding to the anatase (1 0 1), (1 0 3), (2 0 0), (1 0 5), and (2 1 3) planes, respectively. No rutile peaks were detected. In the diffraction patterns of the gold-loaded catalysts additional peaks appear at 44.3° and 64.6°, which were respectively attributed to the (2 0 0) and (2 2 0) reflections in metallic gold. The size of crystalline regions in the samples were estimated using the Scherrer equation,

$$L = \frac{K\lambda}{\beta cos\theta} \quad \textbf{(1)}$$

where *L* is the minimum size of a crystalline region, *K* is the Scherrer shape factor for the crystal structure equal 0.9, λ is the x-ray wavelength used by the instrument (0.15418 nm), β is the full-width at half-maximum value of a diffraction peak, and θ is the Bragg angle.[55] The anatase crystallite sizes were calculated using the anatase (1 0 1) reflection, and were found to be between 6.9 and 7.2 nm for all catalysts except the 0Au-WO_3-TiO_2, which had a slightly larger crystallite size of 7.6 nm. The gold NP sizes were estimated using the gold (2 0 0) reflection, because the more intense gold (1 1 1) peak is obscured by the anatase (1 0 3) peak. The gold NP sizes were found to be in the range of 5-6 nm for the 3 and 5 weight percent catalysts. The size of the gold NPs were generally larger for the Au-WO_3-TiO_2 catalysts than the corresponding Au-TiO_2 catalysts. This was attributed to sintering of Au NPs that occurred during the additional calcination performed during WO_3 addition to form the ternary catalysts. The gold NP growth due to sintering was most dramatic for the 1 weight percent Au catalysts, which were ~3 nm for the WO_3-free species and increased to ~10 nm after WO_3 addition. The tendency of gold NPs to sinter at temperatures above 400°C has been well documented.[56] No crystalline WO_3 was

observed in the diffraction patterns of the catalysts, which indicates that the WO_3 was well dispersed across the surface of the material. This result is corroborated by the results of a study by Yu et al., which showed that the dispersion of WO_3 on the surface of anatase is strongly related to the amount of WO_3 present, and at loadings lower than 6.9 weight percent WO_3 exists as a highly dispersed species on the surface of the TiO_2.[57]

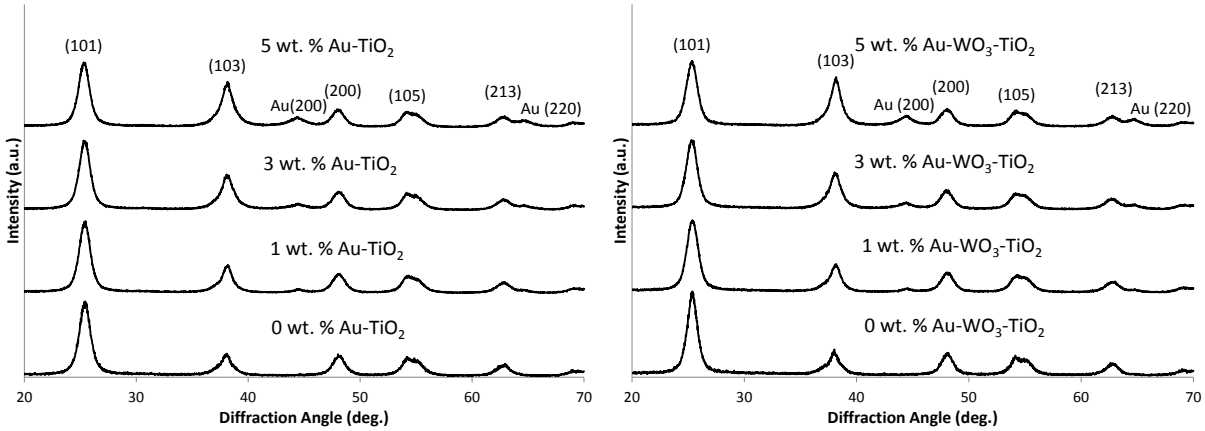

Figure 3. X-ray diffraction patterns for catalysts. All peaks are labeled with the corresponding Miller index, and correspond to anatase TiO_2 unless designated "Au" for the gold peaks.

Photocatalytic Degradation of DMMP

Figure 4 displays the results of the photocatalytic experiments for the Au-TiO_2 and Au-WO_3-TiO_2 catalyst series. The detection limit of the method used is indicated on each graph as a dashed line, and represents 77% degradation. As expected, each of the WO_3 containing catalysts was found to be more efficient in the degradation of DMMP than the corresponding WO_3-free catalyst with similar Au- loading in the Au-TiO_2, with the exception of the 0 weight percent species which displayed similar activity. After 30 hours of irradiation, the 1 and 3 wt. % Au-WO_3-TiO_2 catalysts had fully degraded the DMMP, with final concentration values less than one standard deviation higher than the detection limit for the method (Table 2). The 5 wt. % Au ternary catalyst was only slightly less effective than the 1 and 3 wt. % ternary counterparts, with the final concentration of DMMP more than one standard deviation above

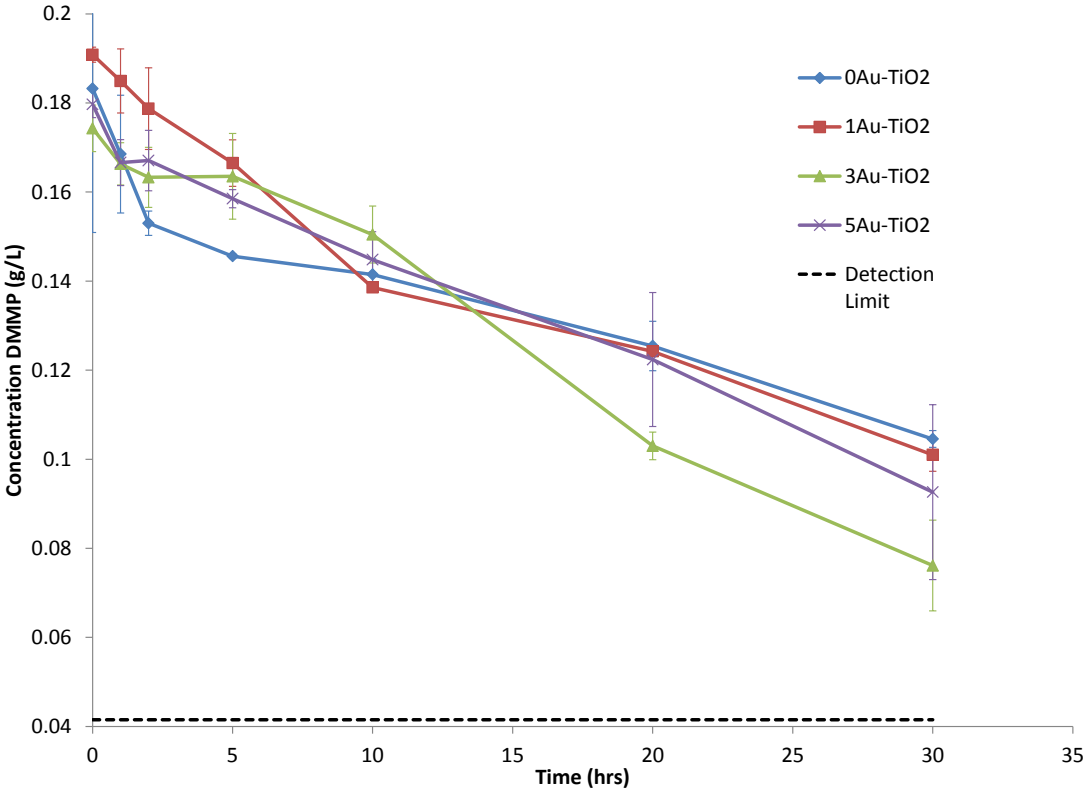

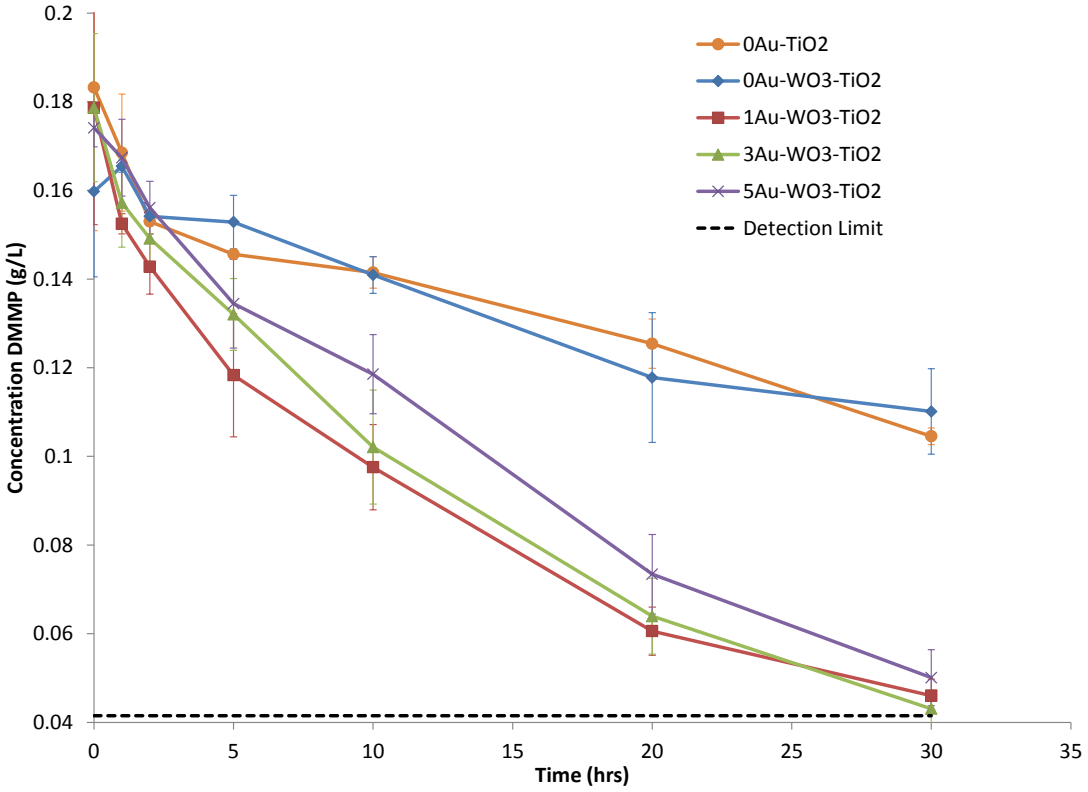

Figure 4. Concentration of DMMP in reaction mixture over 30 hours of irradiation for Au-TiO_2 and Au-WO_3-TiO_2 catalyst series.

Table 2. Final concentration of DMMP after 30 hours of irradiation for each catalyst.

Catalyst	*DMMP Concentration after 30 hours (mg L^{-1})*	*% DMMP Degraded*[a]
0Au-TiO_2	105 ± 2	42%
1Au-TiO_2	101 ± 4	44%
3Au-TiO_2	76 ± 10	57%
5Au-TiO_2	93 ± 20	48%
0Au-WO_3-TiO_2	95 ± 23	39%
1Au-WO_3-TiO_2	44 ± 3	74%
3Au-WO_3-TiO_2	44 ± 3	76%
5Au-WO_3-TiO_2	50 ± 6	72%
Detection Limit:	42	77%

[a] Starting concentration of DMMP = 179 mg L^{-1}

the detection limit. The OP agent and catalyst concentrations in the photocatalytic experiments, 0.25 g L^{-1} and 0.1 g L^{-1}, respectively, were considered to be representative of a system of high-concentration aqueous OP agent contamination. Although increasing the starting concentration of DMMP would lower the lower detection limit with respect to the starting concentration of DMMP, such a high-concentration system was considered to be a poor mimic for a real system of OP compound contaminated water.

The differences in final DMMP concentration for the 0, 1, and 5 wt. % Au-TiO_2 catalysts were not statistically significant. DMMP degradation after 30 hours by the Au-TiO_2 catalysts was identical for all the WO_3-free catalysts except for the 3 wt. % Au species, which was slightly more efficient (final concentration 0.076 g/L) than for the 0Au-TiO_2 (final concentration 0.10 g/L).

The concentration of DMMP was calculated using a standard liquid-liquid extraction procedure with DEMP added as a quantitative extraction standard and analyzed by GCMS with DEEP as a GCMS standard. Figure 5 displays a typical trace for the degradation of DMMP by one of the more active catalysts in the series. The reaction progress was indicated by the disappearance of the DMMP peak. No product peaks were detected for any of the catalysts, indicating that the catalysts mineralized the

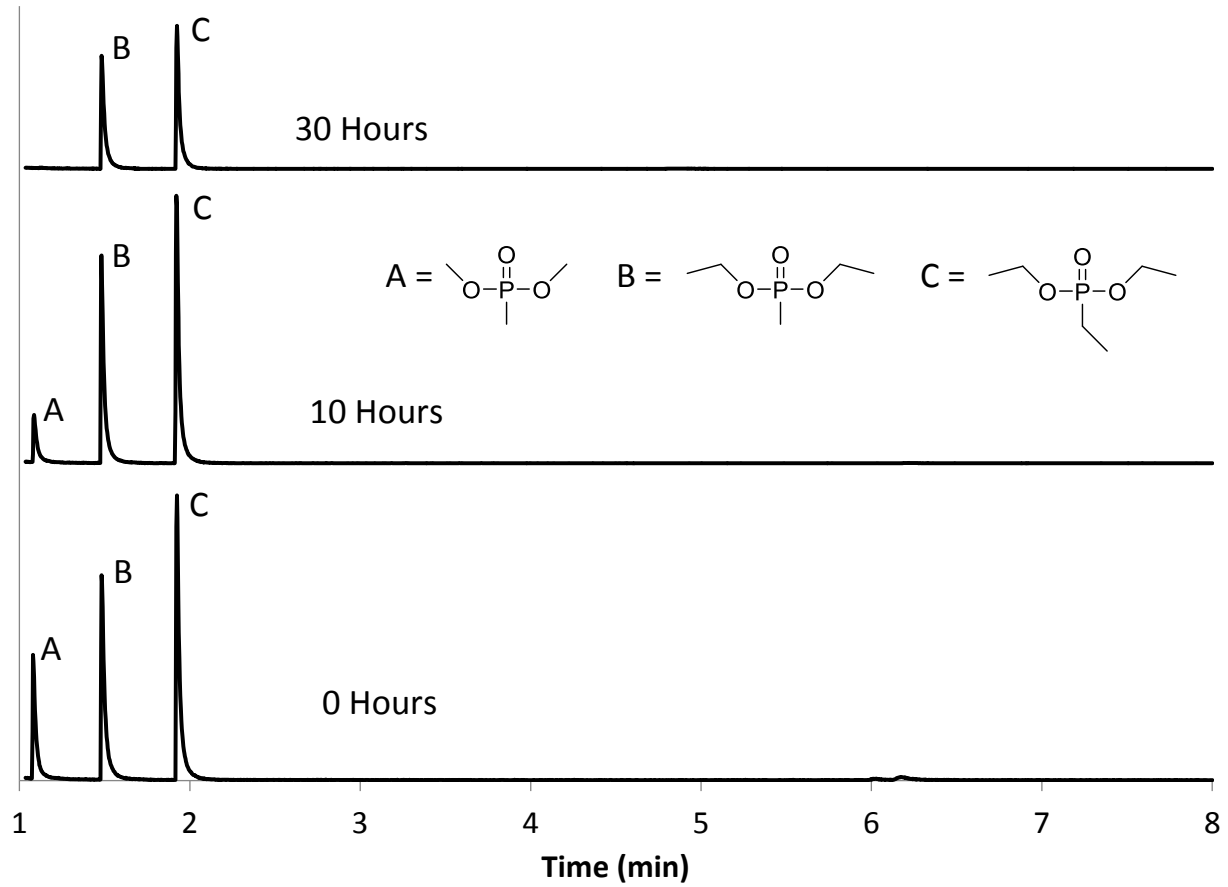

Figure 5. Gas chromatogram of DMMP degradation after 0, 10, and 30 hours of irradiation. Peaks A, B, and C correspond to DMMP, DEMP, and DEEP.

DMMP to inorganic phosphate products.

The results for the efficiency of the catalysts are consistent with previous theories on the effects of both dopants on TiO_2. Au NPs are thought to prevent electron/hole recombination from occurring by facilitating a photoinduced charge transfer of the conduction band electron to the Au NP. The addition of noble metal NPs does not affect the band-gap of a metal oxide semiconductor, which is supported by the similar photocatalytic activity displayed by the Au-TiO_2 catalysts.

The increased photocatalytic activity demonstrated by the ternary catalysts can be attributed to the addition of WO_3 to the material. The addition of WO_3 has been shown to increase the photocatalytic activity of TiO_2 compounds through the combined effects of increasing the adsorption potential of the material by increasing the surface acidity, and increasing the charge separation by trapping excited

electrons.[34, 58] Additionally, Li et al.[37] found that doping TiO_2 with WO_3 could shift the absorption edge to the visible region from the near UV. Although it is apparent that the addition of WO_3 to the Au-TiO_2 catalysts increased their photocatalytic efficiency, it is at present unclear whether the increase was due to a sensitization of the catalyst to visible light, to an increase in the number and strength of the acid sites on the surface of the catalyst, or a combination of the two. Two additional experiments can be performed that will identify the primary cause for the increase in activity. The first experiment is the irradiation of a catalyst-free DMMP solution, which would establish a true zero-photocatalytic activity baseline by which to compare the activity of the Au-TiO_2 and Au-WO_3-TiO_2 series. If the results show a similar decrease in DMMP concentration to the Au-TiO_2 series, then the activity of Au-WO_3-TiO_2 catalysts can be attributed to visible light photocatalysis. However, if the results display no decrease in DMMP concentration, then the photocatalytic degradation may be attributed to either UV or visible light response. Because the acid site strength would only affect the catalyst performance if the UV light was not completely filtered out by the borosilicate glass of the reaction vessel, an additional control experiment can be envisioned where unfiltered light from the xenon short arc lamp is shined directly on the reaction mixture. If the Au-TiO_2 catalysts, which are expected to be UV-light responsive, display similar activities in the unfiltered and the borosilicate glass filtered experiments, then the activity shown by the Au-WO_3-TiO_2 catalyst series can be attributed to UV light response. These results would identify an increase in surface acidity or charge-separation facilitated by WO_3 as the primary cause for the higher photocatalytic activity of the ternary series.

The results for the ternary catalyst series indicate that the concentration of gold NPs on the surface of the TiO_2 does not greatly affect the overall catalytic activity of a species towards the degradation of DMMP within the studied Au weight percent. Additionally, one of the two most active catalysts, 1Au-WO_3-TiO_2, was shown by Scherrer equation calculations to have a gold NP size of 10 nm. Typically, smaller nanoparticle size is associated with higher photocatalytic activity, but despite that the

1Au-WO_3-TiO_2 was one of the most active catalysts. The higher activity displayed by the Au-WO_3-TiO_2 series suggests that although varying the weight percent gold on the catalyst surface does not affect the photocatalytic activity of the species as significantly as expected, the presence of both gold and tungsten oxide on the titania substrate together results in an increase in activity. The presence of WO_3 did not significantly change the activity of the 0 wt.% Au catalysts (0.095 g/L after 30 hours 0Au-WO_3-TiO_2 vs. 0.105 g/L after 30 hours 0Au-TiO_2), but the Au- and WO_3- modified TiO_2 catalysts all degraded more DMMP after 30 hours than the WO_3-free Au-TiO_2 catalysts.

CONCLUSIONS

Porous ternary Au- and WO_3- loaded TiO_2 composites were synthesized by a sonochemical addition of gold nanoparticles and subsequent dry impregnation of WO_3 to TiO_2 microparticles that were replicated from SiO_2. Two series were synthesized, one with just Au and the other with both Au and WO_3, with variable Au loadings of 0, 1, 3, and 5 weight percent for both series, and 4 weight percent WO_3 on the ternary series. The gold nanoparticles were found to be larger on the WO_3-containing series, likely due to sintering during the additional calcination step performed on that series and ranged from 6-10 nm. On the series without WO_3 the gold nanoparticle sizes ranged from 3-5 nm. Crystalline WO_3 was not observed by x-ray diffraction analysis, indicating the species formed a monolayer on the surface of the TiO_2. The visible light photocatalytic activity of the Au-TiO_2 series was compared to the activity of the Au-WO_3-TiO_2 series in the mineralization of an organophosphorus compound, dimethyl methylphosphonate. It was found that the Au-WO_3-TiO_2 series performed significantly better than the Au-TiO_2 series, although the variably quantities of gold NPs had little effect on the efficiency within a series. Both gold-free catalysts, TiO_2 and WO_3-TiO_2, displayed similar degradation efficiencies, leading to the conclusion that the interaction of the three components (TiO_2, WO_3, and Au) contributed to the overall photocatalytic efficiency of a material more than the presence of either individual dopant.

REFERENCES

1. Mika, O. J.; Fiserova, L., *Toxin Rev.* **2011,** *30*, 115-121.
2. Singh, B. K.; Walker, A., *FEMS Microbiol. Rev.* **2006,** *30*, 428-471.
3. Jamal, G. A.; Hansen, S.; Julu, P. O. O., *Toxicology* **2002,** *181-182*, 23-33.
4. Čolović, M. B.; Krstić, D. Z.; Lazarević-Pašti, T. D.; Bondžić, A. M.; Vasić, V. M., *Curr. Neuropharmacol.* **2013,** *11*, 315-335.
5. Sultatos, L. G., *J. Toxicol. Environ. Health* **1994,** *43*, 271-289.
6. Abou-Donia, M. B.; Lapadula, D. M., *Annu. Rev. Pharmacol. Toxicol.* **1990,** *30*, 405-440.
7. Johnson, M. K., *Rev. Biochem. Toxicol.* **1982,** *4*, 141-212.
8. O'Shea, K. E.; Garcia, I.; Aguilar, M., *Res. Chem. Intermed.* **1997,** *23*, 325-339.
9. O'Shea, K. E.; Beightol, S.; Garcia, I.; Aguilar, M.; Kalen, D. V.; Cooper, W. J., *J. Photochem. Photobiol., A* **1997,** *107*, 221-226.
10. O'Shea, K. E., *Mol. Supramol. Photochem.* **2003,** *10*, 231-247.
11. Mera, N.; Hirakawa, T.; Sano, T.; Takeuchi, K.; Seto, Y.; Negishi, N., *J. Hazard. Mater.* **2010,** *177*, 274-280.
12. Kozlova, E. A.; Vorontsov, A. V., *Appl. Catal., B* **2006,** *63*, 114-123.
13. Kozlova, E. A.; Smirniotis, P. G.; Vorontsov, A. V., *J. Photochem. Photobiol., A* **2004,** *162*, 503-511.
14. Yu, J. C.; Yu, J. G.; Ho, W. K.; Jiang, Z. T.; Zhang, L. Z., *Chem. Mater.* **2002,** *14*, 3808-3816.
15. Fujishima, A.; Honda, K., *Nature* **1972,** *238*, 37-38.
16. Jiang, C.; Zhang, J., *J. Mater. Sci. Technol. (Shenyang, China)* **2013,** *29*, 97-122.
17. Fujishima, A.; Rao, T. N.; Tryk, D. A., *J. Photochem. Photobiol., C* **2000,** *1*, 1-21.
18. Hanaor, D. A. H.; Sorrell, C. C., *J. Mater. Sci.* **2011,** *46*, 855-874.
19. Yasutomi, Y., *Hyomen Kagaku* **2013,** *34*, 321-323.
20. Vorontsov, A. V.; Kozlov, D. V.; Smirniotis, P. G.; Parmon, V. N., *Kinet. Catal.* **2005,** *46*, 189-203.
21. Peral, J.; Casado, J.; Domenech, J., *J. Photochem. Photobiol., A* **1988,** *44*, 209-217.
22. Tang, H.; Prasad, K.; Sanjinès, R.; Schmid, P. E.; Lévy, F., *J. Appl. Phys.* **1994,** *75*, 2042-2047.
23. Umebayashi, T.; Yamaki, T.; Itoh, H.; Asai, K., *Appl. Phys. Lett.* **2002,** *81*, 454-456.
24. Sathish, M.; Viswanathan, B.; Viswanath, R. P.; Gopinath, C. S., *Chem. Mater.* **2005,** *17*, 6349-6353.
25. Kwon, Y. T.; Song, K. Y.; Lee, W. I.; Choi, G. J.; Do, Y. R., *J. Catal.* **2000,** *191*, 192-199.
26. Do, Y. R.; Lee, W.; Dwight, K.; Wold, A., *J. Solid State Chem.* **1994,** *108*, 198-201.
27. Ramos-Delgado, N. A.; Gracia-Pinilla, M. A.; Maya-Trevino, L.; Hinojosa-Reyes, L.; Guzman-Mar, J. L.; Hernandez-Ramirez, A., *J. Hazard. Mater.* **2013,** *263*, 36-44.
28. Ranjit, K. T.; Viswanathan, B., *J. Photochem. Photobiol., A* **1997,** *108*, 79-84.
29. Pena, D. A.; Uphade, B. S.; Smirniotis, P. G., *J. Catal.* **2004,** *221*, 421-431.
30. Kaur, R.; Pal, B., *J. Mol. Catal. A: Chem.* **2012,** *355*, 39-43.
31. Zhu, B.; Li, K.; Zhou, J.; Wang, S.; Zhang, S.; Wu, S.; Huang, W., *Catal. Commun.* **2008,** *9*, 2323-2326.
32. Nagaveni, K.; Hegde, M. S.; Ravishankar, N.; Subbanna, G. N.; Madras, G., *Langmuir* **2004,** *20*, 2900-2907.
33. Serpone, N., *J. Phys. Chem. B* **2006,** *110*, 24287-24293.
34. Onfroy, T.; Lebarbier, V.; Clet, G.; Houalla, M., *J. Mol. Catal. A: Chem.* **2010,** *318*, 1-7.
35. Kresge, C. T.; Leonowicz, M. E.; Roth, W. J.; Vartuli, J. C.; Beck, J. S., *Nature (London)* **1992,** *359*, 710-712.
36. Nair, M. M.; Yen, H.; Kleitz, F., *C. R. Chim.* **2014,** *17*, 641-655.
37. Li, X. Z.; Li, F. B.; Yang, C. L.; Ge, W. K., *J. Photochem. Photobiol., A* **2001,** *141*, 209-217.
38. Ke, D. N.; Liu, H. J.; Peng, T. Y.; Liu, X.; Dai, K., *Mater. Lett.* **2008,** *62*, 447-450.

39. Riboni, F.; Bettini, L. G.; Bahnemann, D. W.; Selli, E., *Catal. Today* **2013,** *209*, 28-34.
40. Sajjad, A. K. L.; Shamaila, S.; Tian, B.; Chen, F.; Zhang, J., *Appl. Catal., B* **2009,** *91*, 397-405.
41. Yang, D.; Park, S.-E.; Lee, J.-K.; Lee, S.-W., *J. Cryst. Growth* **2009,** *311*, 508-511.
42. Chen, X.; Mao, S. S., *Chem. Rev.* **2007,** *107*, 2891-2959.
43. Kumar, S. G.; Devi, L. G., *J. Phys. Chem. A* **2011,** *115*, 13211-13241.
44. Pol, V. G.; Gedanken, A.; Calderon-Moreno, J., *Chem. Mater.* **2003,** *15*, 1111-1118.
45. Iliev, V.; Tomova, D.; Rakovsky, S.; Eliyas, A.; Puma, G. L., *J. Mol. Catal. A: Chem.* **2010,** *327*, 51-57.
46. Karacsonyi, E.; Baia, L.; Dombi, A.; Danciu, V.; Mogyorosi, K.; Pop, L. C.; Kovacs, G.; Cosoveanu, V.; Vulpoi, A.; Simon, S.; Pap, Z., *Catal. Today* **2013,** *208*, 19-27.
47. Kovacs, G.; Baia, L.; Vulpoi, A.; Radu, T.; Karacsonyi, E.; Dombi, A.; Hernadi, K.; Danciu, V.; Simon, S.; Pap, Z., *Appl. Catal., B* **2014,** *147*, 508-517.
48. Gallis, K. W.; Araujo, J. T.; Duff, K. J.; Moore, J. G.; Landry, C. C., *Adv. Mater. (Weinheim, Ger.)* **1999,** *11*, 1452-1455.
49. Leitner, A.; Sturm, M.; Hudecz, O.; Mazanek, M.; Smått, J.-H.; Lindén, M.; Lindner, W.; Mechtler, K., *Anal. Chem.* **2010,** *82*, 2726-2733.
50. DePuccio, D. P.; Botella, P.; O'Rourke, B.; Landry, C. C., *ACS Appl. Mater. Interfaces* **2015,** *7*, 1987-1996.
51. Brunauer, S.; Emmett, P. H.; Teller, E., *J. Am. Chem. Soc.* **1938,** *60*, 309-319.
52. Barrett, E. P.; Joyner, L. G.; Halenda, P. P., *J. Am. Chem. Soc.* **1951,** *73*, 373-380.
53. Sclafani, A.; Herrmann, J. M., *J. Phys. Chem.* **1996,** *100*, 13655-13661.
54. Luttrell, T.; Halpegamage, S.; Tao, J.; Kramer, A.; Sutter, E.; Batzill, M., *Sci. Rep.* **2014,** *4*, 4043/4041-4043/4048.
55. Patterson, A. L., *Phys. Rev.* **1939,** *56*, 978-982.
56. Tsubota, S.; Nakamura, T.; Tanaka, K.; Haruta, M., *Catal. Lett.* **1998,** *56*, 131-135.
57. Yu, X.-F.; Wu, N.-Z.; Huang, H.-Z.; Xie, Y.-C.; Tang, Y.-Q., *J. Mater. Chem.* **2001,** *11*, 3337-3342.
58. Zhang, H.; Chen, G.; Bahnemann, D. W., *J. Mater. Chem.* **2009,** *19*, 5089-5121.